Generalized coupled-mode theory for $\chi^{(2)}$ interactions in finite multilayered structures

Giuseppe D'Aguanno and Marco Centini

Dipartimento di Energetica, Istituto Nazionale di Fisica della Materia, Università di Roma "La Sapienza," Via A. Scarpa 16, I-00161 Rome, Italy, and Weapons Sciences Directorate, Research Development and Engineering Center, U.S. Army Aviation and Missile Command, Building 7804, Redstone Arsenal, Alabama 35898-5000

Michael Scalora

Weapons Sciences Directorate, Research Development and Engineering Center, U.S. Army Aviation and Missile Command, Building 7804, Redstone Arsenal, Alabama 35898-5000

Concita Sibilia and Mario Bertolotti

Dipartimento di Energetica, Istituto Nazionale di Fisica della Materia, Università di Roma "La Sapienza," Via A. Scarpa 16, I-00161 Rome, Italy

Mark J. Bloemer and Charles M. Bowden

Weapons Sciences Directorate, Research Development and Engineering Center, U.S. Army Aviation and Missile Command, Building 7804, Redstone Arsenal, Alabama 35898-5000

Received December 7, 2001; revised manuscript March 5, 2002

Using a first-order multiple-scale expansion approach, we derive a set of coupled-mode equations that describe both forward and backward second-harmonic generation and amplification processes in nonlinear, one-dimensional, multilayered structures of finite length. The theory is valid for index modulation of arbitrary depth and profile. We derive analytical solutions in the undepleted pump regime under different pumping circumstances. The model shows excellent agreement with the numerical integration of Maxwell's equations.

OCIS codes: 190.4410, 230.4170.

1. INTRODUCTION

The nonlinear quadratic response in finite, one-dimensional (1-D), photonic bandgap (PBG) structures with deep gratings can be enhanced by several orders of magnitude with respect to an equivalent length of a bulk material owing to the simultaneous availability of high field localization, i.e., high density of modes (DOM) and exact phase-matching conditions near the photonic band edge.[1–7] However, a formal theory that describes nonlinear quadratic interactions in finite, 1-D structures with arbitrary index-modulation depth is still lacking. Therefore our aim is to present a generalized coupled-mode theory that applies to this case.

Current approaches can be summarized as follows: (a) the coupled-mode theory[8] or the Green's function approach[9] for finite, periodic, shallow gratings, and (b) Bloch mode expansion[10,11] or a generalized coupled-mode theory[12] for infinite, periodic, deep gratings that are used mostly within the context of solitonlike pulses (often referred to as gap solitons) in cubic $\chi^{(3)}$ and quadratic $\chi^{(2)}$ media. In the situations studied in Refs. 1–7 the spatial extension of incident pulses exceeds the spatial extension of a typical structure by several orders of magnitude.[1,7] In this case, field localization resulting from cavity effects plays a crucial role in the enhancement of the nonlinear response, and boundary conditions at the input and the output interfaces have to be taken into account explicitly. These circumstances are not the same as those that are typically considered in Refs. 10–12, for example, in which the structure is much longer compared with the spatial extension of the pulse.

This paper is organized as follows: In Section 2, we first discuss some key properties of the electromagnetic modes in a linear grating and find a suitable basis of expansion. Then we perform a first-order multiple-scale expansion and derive a set of coupled-mode equations. In Section 3, we use the coupled-mode equations derived in Section 2 to study different regimes under the undepleted pump approximation, namely, (a) second-harmonic generation (SHG), and (b) second harmonics (SHs) generated by counterpropagating pump fields. In Section 4, we apply the theory to the case of SHG in a single material layer. In Section 5, we apply the theory to the case of resonant interaction in nonabsorbing, finite, PBG struc-

tures. We derive simple analytical solutions that show excellent agreement with the full numerical integration of Maxwell's equations, as verified in Section 6.

2. COUPLED-MODE EQUATIONS

The condition in which an incident pulse may be orders of magnitude longer than the spatial extension of the structure is equivalent to stating that the spectral bandwidth of the pulse is much narrower with respect to any of the transmission resonances of the structure. This relation allows us to neglect the temporal dynamics and to write the solution of the wave equation in the form of monochromatic waves: $E_j(z, t) = E_{j\omega}(z)\exp[-i(j\omega)t]$, as outlined at length in Ref. 7. Although at first sight the monochromatic approximation might seem to be a rather severe restriction, in reality for the typical multilayered structures that we consider the monochromatic regime is quickly approached with input pulses that are only a few picoseconds in duration—see Fig. 1.

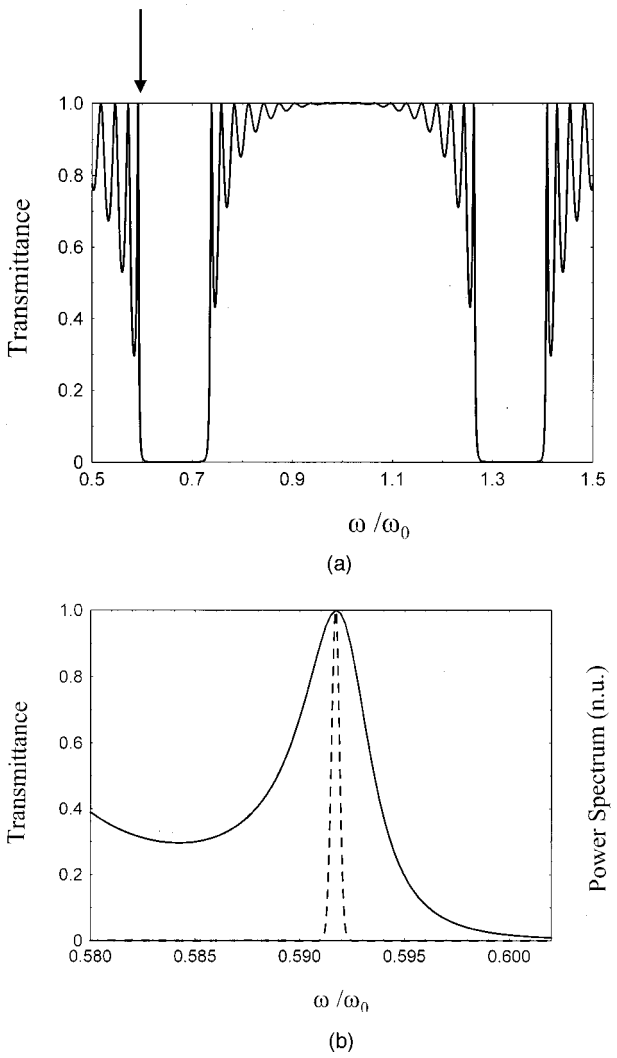

Fig. 1. (a) Transmittance plotted versus the normalized frequency for a typical structure made of a half–quarter-wave stack. The structure is composed of 39 alternating layers of high and low refractive index. The indices of refraction of the layers are, respectively: $n_1 = 1.4285$ and $n_2 = 1$. The layers have thicknesses of $a = \lambda_0/(2n_1)$ and $b = \lambda_0/(4n_2)$, where $\lambda_0 = 1\ \mu$m and $\omega_0 = 2\pi c/\lambda_0$; the total length of the structure is $L = 11.75\ \mu$m. The arrow identifies the first transmission resonance near the first-order bandgap. (b) Magnification of the first transmission resonance (solid curve) near the first-order bandgap. Also shown is the power spectrum (dashed curve) of a Gaussian input pulse of 2 ps in duration with its carrier frequency tuned to the first transmission resonance. Note that the spectral bandwidth of the pulse is approximately 1 order of magnitude narrower than the spectral bandwidth of the transmission resonance. This is a typical situation in which the interaction can be described by monochromatic waves.

If we assume the rotating-wave approximation the equations governing nonlinear quadratic interactions of two monochromatic plane waves at the fundamental frequency (FF) ω and the SH frequency 2ω in a layered, 1-D, finite structure can be written as[4]

$$\frac{d^2E_\omega}{dz^2} + \frac{\omega^2\epsilon_\omega(z)}{c^2}E_\omega = -2\frac{\omega^2}{c^2}d^{(2)}(z)E_\omega^*E_{2\omega}, \quad (1a)$$

$$\frac{d^2E_{2\omega}}{dz^2} + \frac{4\omega^2\epsilon_{2\omega}(z)}{c^2}E_{2\omega} = -4\frac{\omega^2}{c^2}d^{(2)}(z)E_\omega^{\,2}, \quad (1b)$$

where $\epsilon_{j\omega}(z)$, $j = 1, 2$, are the spatially dependent, dielectric functions for the FF and the SH fields. In general, $\epsilon_{j\omega}(z)$ are assumed to be complex functions. The condition $\epsilon_\omega(z) \neq \epsilon_{2\omega}(z)$ takes into account possible material dispersion. Finally, $d^{(2)}(z)$ is the spatially dependent quadratic coupling function.

Before considering the full nonlinear problem, we discuss some key properties of the electromagnetic modes in a linear grating. Let us begin with the Helmholtz equation for a monochromatic plane wave oscillating at frequency ω:

$$\frac{d^2E_{j\omega}}{dz^2} + \frac{(j\omega)^2\epsilon_{j\omega}(z)}{c^2}E_{j\omega} = 0. \quad (2)$$

For a finite grating of length L located between $z = 0$ and $z = L$ the general solution of Eq. (2) between $z = 0$ and $z = L$ can be expressed as a linear superposition of the left-to-right (LTR) and the right-to-left (RTL) propagating modes, as in[13]

$$E_{j\omega}(z) = A_\omega^{(+)}\Phi_{j\omega}^{(+)}(z) + A_{j\omega}^{(-)}\Phi_{j\omega}^{(-)}(z), \quad (3)$$

where $A_{j\omega}^{(+)}$ is the amplitude of the electric field incident from LTR and $A_{j\omega}^{(-)}$ is the electric field amplitude incident from RTL (see Fig. 2). The LTR and the RTL modes $\Phi_{j\omega}^{(\pm)}(z)$ can be calculated by use of the standard matrix-transfer technique[14] and satisfy the usual boundary conditions (see Fig. 2). In what follows, we can define a metric by using the following scalar product:

$$\langle f|g\rangle \equiv \frac{1}{L}\int_0^L f^*(z)g(z)dz.$$

In general $\Phi_{j\omega}^{(\pm)}(z)$ are not orthogonal. We may redefine a more convenient orthogonal system of functions by using a standard orthogonalization procedure. This approach allows us to express the general solution of the Helmholtz equation in terms of a new orthogonal set of functions $[\Phi_{j\omega}^{(+)}, U_{j\omega}^{(-)}]$ as

$$E_{j\omega}(z) = B_{j\omega}^{(+)}\Phi_{j\omega}^{(+)}(z) + A_{j\omega}^{(-)}U_{j\omega}^{(-)}(z), \quad (4)$$

where

$$B_{j\omega}^{(+)} = A_{j\omega}^{(+)} + \beta_{j\omega} A_{j\omega}^{(-)}, \tag{5a}$$

$$U_{j\omega}^{(-)}(z) = \Phi_{j\omega}^{(-)}(z) - \beta_{j\omega}\Phi_{j\omega}^{(+)}, \tag{5b}$$

$$\beta_{j\omega} = \frac{\langle \Phi_{j\omega}^{(+)} | \Phi_{j\omega}^{(-)} \rangle}{\langle \Phi_{j\omega}^{(+)} | \Phi_{j\omega}^{(+)} \rangle}. \tag{5c}$$

We chose to represent the solution of the Helmholtz equation in terms of an orthogonal set of functions because that allows us to perform the projection of the perturbed nonlinear equations in a consistent way.

Now we return to the full nonlinear equations (1). The physical idea that will guide us in looking for solutions of Eqs. (1) can be expressed as follows: We assume that the effect of the nonlinearity in Eqs. (1) is to modulate the solution of the linear problem on a length scale that is much longer with respect to the length scale over which modulation of the linear solution occurs. Therefore we apply a multiple-scale expansion[10,15] by introducing a new set of independent variables: $z_\alpha = \lambda^\alpha z$, with $\alpha = 0,1,2,\ldots$. The relation $\lambda \ll 1$ is a dimensionless expansion parameter that allows us to separate fast and slow scale variations. At the end of the multiple-scale approach, we formally take the limit $\lambda \to 1$ to restore the original space variable z. We point out that the use of the expansion parameter λ does not imply any kind of assumption about the order of magnitude of the nonlinear coefficient $d^{(2)}$. The effect of the parameter λ is to allow the separation of fast and slow scale variations in the spatial dynamics of the nonlinear equations. The use of the multiple-scale expansion approach is based on only the hypothesis of the existence of different-length scales of variation as the dynamics evolve.

The linear and the nonlinear dielectric functions, $\epsilon_{j\omega}(z)$ and $d^{(2)}(z)$, respectively, are considered as functions of the fast variable z_0. The field envelope functions, which we introduce below, are functions of the slowly varying variables z_1, z_2, and so forth. The multiple-scale procedure calls for the expansion of the derivative operator in terms of the new set of coordinates:

$$\frac{\mathrm{d}}{\mathrm{d}z} = \frac{\partial}{\partial z_0} + \lambda \frac{\partial}{\partial z_1} + \lambda^2 \frac{\partial}{\partial z_2} + \ldots. \tag{6}$$

The electric fields are also expanded in powers of the perturbing parameter λ in a self-consistent manner:

$$E_{j\omega} = \lambda E_{j\omega}^{(1)}(z_0, z_1, z_2, \ldots) + \lambda^2 E_{j\omega}^{(2)}(z_0, z_1, z_2, \ldots) + \ldots, \qquad j = 1,2. \tag{7}$$

Substituting Eqs. (6) and (7) into Eqs. (1a) and (1b) and collecting the terms proportional to λ, we find

$$\frac{\partial^2 E_{j\omega}^{(1)}}{\partial {z_0}^2} = -\frac{(j\omega)^2}{c^2}\epsilon_{j\omega}(z_0) E_{j\omega}^{(1)}, \qquad j = 1,2. \tag{8}$$

In accord with our discussion above, solutions of Eq. (8) can be expressed [see Eq. (3)] as

$$E_{j\omega}^{(1)} = B_{j\omega}^{(+)}(z_1, z_2, \ldots)\Phi_{j\omega}^{(+)}(z_0) + A_{j\omega}^{(-)}(z_1, z_2, \ldots)U_{j\omega}^{(-)}(z_0), \tag{9}$$

where $B_{j\omega}^{(+)}(z_1, z_2, \ldots)$ and $A_{j\omega}^{(-)}(z_1, z_2, \ldots)$ are field envelopes that depend on the slow variables $(z_1, z_2, \ldots)$. Collecting the terms proportional to λ^2, we find

$$\left[\frac{\partial^2}{\partial {z_0}^2} + \frac{\omega^2 \epsilon_\omega(z_0)}{c^2}\right] E_\omega^{(2)} + 2\frac{\partial}{\partial z_0}\frac{\partial}{\partial z_1} E_\omega^{(1)} = -2\frac{\omega^2}{c^2} d^{(2)}(z_0) E_\omega^{(1)*} E_{2\omega}^{(1)}, \tag{10a}$$

$$\left[\frac{\partial^2}{\partial {z_0}^2} + \frac{4\omega^2 \epsilon_{2\omega}(z_0)}{c^2}\right] E_{2\omega}^{(2)} + 2\frac{\partial}{\partial z_0}\frac{\partial}{\partial z_1} E_{2\omega}^{(1)} = -\frac{4\omega^2}{c^2} d^{(2)}(z_0)[E_\omega^{(1)}]^2. \tag{10b}$$

To solve Eqs. (10a) and (10b), we expand the fields $E_{j\omega}^{(2)}$ as

$$E_{j\omega}^{(2)} = C_{j\omega}^{(+)}(z_1, z_2, \ldots)\Phi_{j\omega}^{(+)}(z_0) + C_{j\omega}^{(-)}(z_1, z_2, \ldots)U_{j\omega}^{(-)}(z_0), \tag{11}$$

where $C_{j\omega}^{(\pm)}(z_1, z_2, \ldots)$ are a new set of envelope functions. Substituting Eqs. (9) and (11) into Eqs. (10), we arrive at the following set of equations:

$$2\left[\frac{\partial \Phi_\omega^{(+)}}{\partial z_0}\right]\left[\frac{\partial B_\omega^{(+)}}{\partial z_1}\right] + 2\left[\frac{\partial U_\omega^{(-)}}{\partial z_0}\right]\left[\frac{\partial A_\omega^{(-)}}{\partial z_1}\right] = -2\frac{\omega^2}{c^2} d^{(2)}[B_{2\omega}^{(+)} B_\omega^{(+)*} \Phi_{2\omega}^{(+)} \Phi_\omega^{(+)*} + B_{2\omega}^{(+)} A_\omega^{(-)*} \Phi_{2\omega}^{(+)} U_\omega^{(-)*} + A_{2\omega}^{(-)} B_\omega^{(+)*} U_{2\omega}^{(-)} \Phi_\omega^{(+)*} + A_{2\omega}^{(-)} A_\omega^{(-)*} U_\omega^{(-)*} U_{2\omega}^{(-)}], \tag{12a}$$

$$2\left[\frac{\partial \Phi_{2\omega}^{(+)}}{\partial z_0}\right]\left[\frac{\partial B_{2\omega}^{(+)}}{\partial z_1}\right] + 2\left[\frac{\partial U_{2\omega}^{(-)}}{\partial z_0}\right]\left[\frac{\partial A_{2\omega}^{(-)}}{\partial z_1}\right] = -4\frac{\omega^2}{c^2} d^{(2)}[{B_\omega}^{(+)^2} {\Phi_\omega}^{(+)2} + {A_\omega}^{(-)2} {U_\omega}^{(-)^2} + 2{B_\omega}^{(+)} {A_\omega}^{(-)} {U_\omega}^{(-)} {\Phi_\omega}^{(+)}]. \tag{12b}$$

We now (a) project Eqs. (12) over the orthogonal functions $\Phi_{j\omega}^{(+)}$ and $U_{j\omega}^{(-)}$; (b) use Eqs. (5) to restore the original envelope functions $A_{j\omega}^{(\pm)}(z_1, z_2, \ldots)$, and (c) take the limit $\lambda \to 1$ to restore the original spatial variable z. After straightforward but tedious calculations, we arrive at four coupled nonlinear differential equations,

$$\sum_{l=+,-} p_\omega^{(+,l)} \frac{\mathrm{d}A_\omega^{(l)}}{\mathrm{d}z} = i\frac{\omega}{c} \sum_{(k,l)=(+,-)} \Gamma_{(\omega,+)}^{(k,l)} A_{2\omega}^{(k)} A_\omega^{(l)*}, \tag{13a}$$

$$\sum_{l=+,-} p_\omega^{(-,l)} \frac{\mathrm{d}A_\omega^{(l)}}{\mathrm{d}z} = i\frac{\omega}{c} \sum_{(k,l)=(+,-)} \Gamma_{(\omega,-)}^{(k,l)} A_{2\omega}^{(k)} A_\omega^{(l)*}, \tag{13b}$$

$$\sum_{l=+,-} p_{2\omega}^{(+,l)} \frac{\mathrm{d}A_{2\omega}^{(l)}}{\mathrm{d}z} = i\frac{\omega}{c} \sum_{(k,l)=(+,-)} \Gamma_{(2\omega,+)}^{(k,l)} A_\omega^{(k)} A_\omega^{(l)}, \tag{13c}$$

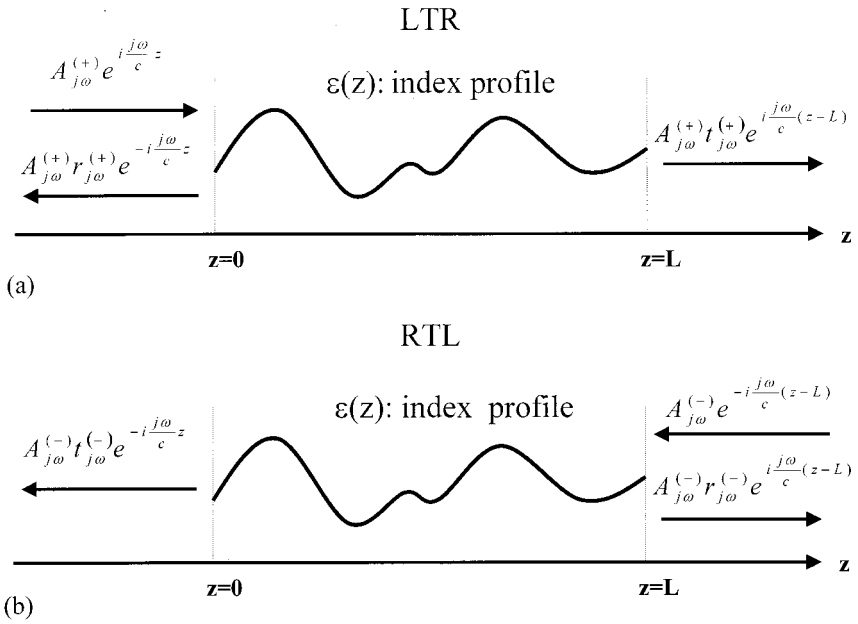

Fig. 2. Schematic representation of the boundary conditions imposed on: (a) the LTR and (b) the RTL modes. The terms $r_{j\omega}^{(\pm)}$ are the LTR and the RTL reflection coefficients, respectively, and $t_{j\omega}^{(\pm)}$ is the transmission coefficient. We find that $t_{j\omega}^{(+)} = t_{j\omega}^{(-)} = t_{j\omega}$ for a nonabsorbing structure as a consequence of time-reversal symmetry.

$$\sum_{l=+,-} p_{2\omega}^{(-,l)} \frac{\mathrm{d}A_{2\omega}^{(l)}}{\mathrm{d}z} = i\frac{\omega}{c} \sum_{(k,l)=(+,-)} \Gamma_{(2\omega,-)}^{(k,l)} A_{\omega}^{(k)} A_{\omega}^{(l)}, \tag{13d}$$

where

$$p_{j\omega}^{(k,l)} = \langle \Phi_{j\omega}^{(k)} | \hat{p}_{j\omega} \Phi_{j\omega}^{(l)} \rangle, \quad \text{for } j = 1, 2 \text{ and } k, l = +, -, \tag{14a}$$

$$\Gamma_{(\omega,n)}^{(k,l)} = \langle \Phi_{\omega}^{(n)} | d^{(2)} \Phi_{2\omega}^{(k)} \Phi_{\omega}^{(l)*} \rangle, \quad \text{for } n, k, l = +, -, \tag{14b}$$

$$\Gamma_{(2\omega,n)}^{(k,l)} = \langle \Phi_{2\omega}^{(n)} | d^{(2)} \Phi_{\omega}^{(k)} \Phi_{\omega}^{(l)} \rangle, \quad \text{for } n, k, l = +, -. \tag{14c}$$

The variables $p_{j\omega}^{(k,l)}$ are the matrix elements of the momentum operator $\hat{p}_{j\omega} \equiv -i(c/j\omega)(\mathrm{d}/\mathrm{d}z)$ that is calculated for the RTL and the LTR modes, $\{\Phi_{j\omega}^{(\pm)}\}$. The overlap coefficients $\Gamma_{(j\omega,n)}^{(k,l)}$ are effective, complex coupling coefficients that reflect the way in which the LTR and the RTL modes sample the distribution of the nonlinearity $d^{(2)}(z)$ over the structure. The values of $\Gamma_{(j\omega,n)}^{(k,l)}$ are maximized and can be greater than the magnitude of $d^{(2)}(z)$, when the fields interact coherently inside the structure. The phase-matching conditions, therefore, do not appear explicitly in the dynamical equations that govern the interaction. Rather, phase-matching conditions appear in the form of effective, complex coupling coefficients. Because no assumptions were made regarding the type of grating, Eqs. (13) are valid for arbitrary index profiles.

3. UNDEPLETED PUMP APPROXIMATION

A. Second-Harmonic Generation

Let us first consider the case of a field at the FF that is incident at the input surface ($z = 0$) of the structure, and let us assume that the FF field generates a SH signal with negligible depletion. The fact that the pump remains undepleted is equivalent to stating that $A_{\omega}^{(+)}(z) \cong A_{\omega}^{(+)}(0)$ and $A_{\omega}^{(-)}(z) \cong 0$. From Eqs. (13) it follows that

$$p_{2\omega}^{(+,+)} \frac{\mathrm{d}A_{2\omega}^{(+)}}{\mathrm{d}z} + p_{2\omega}^{(+,-)} \frac{\mathrm{d}A_{2\omega}^{(-)}}{\mathrm{d}z} = i\frac{\omega}{c} \Gamma_{(2\omega,+)}^{(+,+)} [A_{\omega}^{(+)}(0)]^2, \tag{15a}$$

$$p_{2\omega}^{(-,+)} \frac{\mathrm{d}A_{2\omega}^{(+)}}{\mathrm{d}z} + p_{2\omega}^{(-,-)} \frac{\mathrm{d}A_{2\omega}^{(-)}}{\mathrm{d}z} = i\frac{\omega}{c} \Gamma_{(2\omega,-)}^{(+,+)} [A_{\omega}^{(+)}(0)]^2. \tag{15b}$$

Because we are considering generation, the boundary conditions on the SH field are as follows: $A_{2\omega}^{(+)}(0) = 0$ and $A_{2\omega}^{(-)}(L) = 0$. Equations (15) can then be easily solved:

$$A_{2\omega}^{(+)}(z) = i\frac{\omega}{c} [A_{\omega}^{(+)}(0)]^2 \frac{\Gamma_{(2\omega,+)}^{(+,+)} p_{2\omega}^{(-,-)} - \Gamma_{(2\omega,-)}^{(+,+)} p_{2\omega}^{(+,-)}}{p_{2\omega}^{(+,+)} p_{2\omega}^{(-,-)} - p_{2\omega}^{(+,-)} p_{2\omega}^{(-,+)}} z, \tag{16a}$$

$$A_{2\omega}^{(-)}(z) = i\frac{\omega}{c} [A_{\omega}^{(+)}(0)]^2 \frac{\Gamma_{(2\omega,-)}^{(+,+)} p_{2\omega}^{(+,+)} - \Gamma_{(2\omega,+)}^{(+,+)} p_{2\omega}^{(-,+)}}{p_{2\omega}^{(+,+)} p_{2\omega}^{(-,-)} - p_{2\omega}^{(+,-)} p_{2\omega}^{(-,+)}} \times (z - L). \tag{16b}$$

We note that forward and backward SHG in the undepleted pump regime depends on the product between the matrix elements of the momentum operator and the overlap integrals. In the subsections that follow, we give examples of applications of Eqs. (16) to specific situations.

B. Second-Harmonic Generation by Use of Counterpropagating Beams

Let us consider two pump fields at FF that are injected from the left and from the right of the structure. From Eqs. (13) the undepleted pump approximation imposes

the conditions $A_\omega^{(+)}(z) \cong A_\omega^{(+)}(0)$ and $A_\omega^{(-)}(z) \cong A_\omega^{(-)}(L)$. We then obtain the following equations:

$$p_{2\omega}^{(+,-)}\frac{dA_{2\omega}^{(+)}}{dz} + p_{2\omega}^{(+,-)}\frac{dA_{2\omega}^{(-)}}{dz} = i\frac{\omega}{c}\{\Gamma_{(2\omega,+)}^{(+,+)}[A_\omega^{(+)}(0)]^2 + \Gamma_{(2\omega,+)}^{(-,-)}[A_\omega^{(-)}(L)]^2 + 2\Gamma_{(2\omega,+)}^{(+,-)}A_\omega^{(+)}(0)A_\omega^{(-)}(L)\}, \tag{17a}$$

$$p_{2\omega}^{(-,+)}\frac{dA_{2\omega}^{(+)}}{dz} + p_{2\omega}^{(-,-)}\frac{dA_{2\omega}^{(-)}}{dz} = i\frac{\omega}{c}\{\Gamma_{(2\omega,-)}^{(+,+)}[A_\omega^{(+)}(0)]^2 + \Gamma_{(2\omega,-)}^{(-,-)}[A_\omega^{(-)}(L)]^2 + 2\Gamma_{(2\omega,-)}^{(+,-)}A_\omega^{(+)}(0)A_\omega^{(-)}(L)\}. \tag{17b}$$

With the initial conditions $A_{2\omega}^{(+)}(0) = 0$ and $A_{2\omega}^{(-)}(L) = 0$, the solutions of Eqs. (17) can be written as

$$A_{2\omega}^{(+)}(z) = i\frac{\omega z}{c[p_{2\omega}^{(+,+)}p_{2\omega}^{(-,-)} - p_{2\omega}^{(+,-)}p_{2\omega}^{(-,+)}]}\{[A_\omega^{(+)} \times (0)]^2[\Gamma_{(2\omega,+)}^{(+,+)}p_{2\omega}^{(-,-)} - \Gamma_{(2\omega,-)}^{(+,+)}p_{2\omega}^{(+,-)}] + [A_\omega^{(-)}(L)]^2[\Gamma_{(2\omega,+)}^{(-,-)}p_{2\omega}^{(-,-)} - \Gamma_{(2\omega,-)}^{(-,-)}p_{2\omega}^{(+,-)}] + 2A_\omega^{(+)}(0)A_\omega^{(-)}(L)[\Gamma_{(2\omega,+)}^{(+,-)}p_{2\omega}^{(-,-)} - \Gamma_{(2\omega,-)}^{(+,-)}p_{2\omega}^{(+,-)}]\}, \tag{18a}$$

$$A_\omega^{(-)}(z) = i\frac{\omega(z-L)}{c[p_{2\omega}^{(+,+)}p_{2\omega}^{(-,-)} - p_{2\omega}^{(+,-)}p_{2\omega}^{(-,+)}]}\{[A_\omega^{(+)} \times (0)]^2[\Gamma_{(2\omega,-)}^{(+,+)}p_{2\omega}^{(+,+)} - \Gamma_{(2\omega,+)}^{(+,+)}p_{2\omega}^{(-,+)}] + [A_\omega^{(-)}(L)]^2[\Gamma_{(2\omega,-)}^{(-,-)}p_{2\omega}^{(+,+)} - \Gamma_{(2\omega,+)}^{(+,+)}p_{2\omega}^{(-,+)}] + 2A_\omega^{(+)}(0)A_\omega^{(-)}(L)[\Gamma_{(2\omega,-)}^{(+,-)}p_{2\omega}^{(+,+)} - \Gamma_{(2\omega,+)}^{(+,-)}p_{2\omega}^{(-,+)}]\}. \tag{18b}$$

We note that, when $A_\omega^{(-)}(L) = 0$, the solutions of Eqs. (18) reduce to the case of SHG by a single pump beam, as in Eqs. (16). Equations (18) can be recast in a more convenient form. In fact, if we write the input amplitudes of the LTR and the RTL pump fields, respectively, as $A_\omega^{(+)}(0) = \{[2I_\omega^{(+,\mathrm{pump})}/\epsilon_0 c]^{1/2}\exp[i\gamma_\omega^{(+)}]\}$ and $A_\omega^{(-)}(L) = \{[2I_\omega^{(-,\mathrm{pump})}/\epsilon_0 c]^{1/2}\exp[i\gamma_\omega^{(-)}]\}$, we obtain

$$A_{2\omega}^{(+)}(z) = i\frac{2\omega z I_\omega^{(+,\mathrm{pump})}\exp[2i\gamma_\omega^{(+)}]}{\epsilon_0 c^2[p_{2\omega}^{(+,+)}p_{2\omega}^{(-,-)} - p_{2\omega}^{(+,-)}p_{2\omega}^{(-,+)}]} \times \{[\Gamma_{(2\omega,+)}^{(+,+)}p_{2\omega}^{(-,-)} - \Gamma_{(2\omega,-)}^{(+,+)}p_{2\omega}^{(+,-)}] + Q\exp(2i\delta\phi_\omega)[\Gamma_{(2\omega,+)}^{(-,-)}p_{2\omega}^{(-,-)} - \Gamma_{(2\omega,-)}^{(-,-)}p_{2\omega}^{(+,-)}] + 2\sqrt{Q}\exp[i\delta\phi_\omega] \times [\Gamma_{(2\omega,+)}^{(+,-)}p_{2\omega}^{(-,-)} - \Gamma_{(2\omega,-)}^{(+,-)}p_{2\omega}^{(+,-)}]\}, \tag{19a}$$

$$A_{2\omega}^{(-)}(z) = i\frac{2\omega(z-L)I_\omega^{(+,\mathrm{pump})}\exp[2i\gamma_\omega^{(+)}]}{\epsilon_0 c^2[p_{2\omega}^{(+,+)}p_{2\omega}^{(-,-)} - p_{2\omega}^{(+,-)}p_{2\omega}^{(-,+)}]} \times \{[\Gamma_{(2\omega,-)}^{(+,+)}p_{2\omega}^{(+,+)} - \Gamma_{(2\omega,+)}^{(+,+)}p_{2\omega}^{(-,+)}] + Q\exp(2i\delta\phi_\omega)[\Gamma_{(2\omega,-)}^{(-,-)}p_{2\omega}^{(+,+)} - \Gamma_{(2\omega,+)}^{(+,+)}p_{2\omega}^{(-,+)}] + 2\sqrt{Q}\exp(i\delta\phi_\omega) \times [\Gamma_{(2\omega,-)}^{(+,-)}p_{2\omega}^{(+,+)} - \Gamma_{(2\omega,+)}^{(+,-)}p_{2\omega}^{(-,+)}]\}, \tag{19b}$$

where $I_\omega^{(\pm,\mathrm{pump})}$ are the input LTR and RTL pump intensities, $\gamma_\omega^{(\pm)}$ are the input phases, $Q = I_\omega^{(-,\mathrm{pump})}/I_\omega^{(+,\mathrm{pump})}$ is the ratio of the input intensities, and $\delta\phi_\omega = \gamma_\omega^{(-)} - \gamma_\omega^{(+)}$ is the phase difference between the input fields. Equations (19) suggest that SHG depends on the ratio of the input intensities and their phase difference. The input intensity ratio and the phase difference of the input fields are, in essence, control parameters that allow enhancement or inhibition of the nonlinear process.

4. SECOND-HARMONIC GENERATION FROM A SINGLE LAYER

As a first application of the theory of Sections 2 and 3, we proceed with the simplest possible example: SH generation from a Fabry–Perot etalon. For a nonabsorbing layer it is possible to evaluate the overlap integrals found in Eqs. (12) analytically. For more complicated structures evaluation of the LTR and the RTL modes $\Phi_{j\omega}^{(\pm)}(z)$ of the linear problem must be done numerically by use of the matrix-transfer technique.[14] This evaluation is then usually followed up with an evaluation of the overlap integrals of Eqs. (14).

Let us suppose that the single layer is composed of an exactly phase-matched quadratic material such that $\epsilon_\omega = \epsilon_{2\omega} = \epsilon$ and that the LTR and the RTL modes for both the pump and the generated signal are tuned to a transmission resonance of the structure. In this case the LTR and the RTL modes can be written as

$$\Phi_{j\omega}^{(+)} = \frac{1}{2}\left(1 + \frac{1}{n}\right)\exp\left(i\frac{jm\pi}{L}z\right) + \frac{1}{2}\left(1 - \frac{1}{n}\right)\exp\left(-i\frac{jm\pi}{L}z\right), \qquad j = 1, 2, \tag{20a}$$

$$\Phi_{j\omega}^{(-)} = \frac{1}{2}\left(1 - \frac{1}{n}\right)\exp\left[i\left(\frac{jm\pi}{L}z + jm\pi\right)\right] + \frac{1}{2}\left(1 + \frac{1}{n}\right) \times \exp\left[-i\left(\frac{jm\pi}{L}z - jm\pi\right)\right], \qquad j = 1, 2, \tag{20b}$$

where L is the thickness of the layer, $n = \sqrt{\epsilon}$ is the refractive index, and $m = 1,2,...$ is an integer that counts the order of the transmission resonance and that also deter-

mines the tuning frequency: $\omega = m\pi c/Ln$. Using Eqs. (20), we then calculate the overlap integrals of Eqs. (14); the coupled-mode equations (13) can be written as

$$\frac{dA_{\omega}^{(+)}}{dz} = i\frac{\omega}{c}\frac{d^{(2)}}{4}\left\{\left(1+\frac{3}{n^2}\right)A_{2\omega}^{(+)}A_{\omega}^{(+)*} + \left(1-\frac{1}{n^2}\right) \times [\exp(-im\pi)A_{2\omega}^{(+)}A_{\omega}^{(-)*} + A_{2\omega}^{(-)}A_{\omega}^{(+)*} + \exp(-im\pi)A_{2\omega}^{(-)}A_{\omega}^{(-)*}]\right\}, \tag{21a}$$

$$\frac{dA_{\omega}^{(-)}}{dz} = -i\frac{\omega}{c}\frac{d^{(2)}}{4}\left\{\left(1-\frac{1}{n^2}\right)\left[\exp(-im\pi)A_{2\omega}^{(+)}A_{\omega}^{(+)*} + A_{2\omega}^{(+)}A_{\omega}^{(-)*} + \exp(-im\pi)A_{2\omega}^{(-)}A_{\omega}^{(+)*} + \left(1+\frac{3}{n^2}\right)A_{2\omega}^{(-)}A_{\omega}^{(-)*}\right]\right\}, \tag{21b}$$

$$\frac{dA_{2\omega}^{(+)}}{dz} = i\frac{\omega}{c}\frac{d^{(2)}}{4}\left\{\left(1+\frac{3}{n^2}\right)A_{\omega}^{(+)2} + \left(1-\frac{1}{n^2}\right) \times [2\exp(im\pi)A_{\omega}^{(+)}A_{\omega}^{(-)} + A_{\omega}^{(-)2}]\right\}, \tag{21c}$$

$$\frac{dA_{2\omega}^{(-)}}{dz} = -i\frac{\omega}{c}\frac{d^{(2)}}{4}\left\{\left(1-\frac{1}{n^2}\right)[A_{\omega}^{(+)2} + 2\exp(im\pi)A_{\omega}^{(+)}A_{\omega}^{(-)}] + \left(1+\frac{3}{n^2}\right)A_{\omega}^{(-)2}\right\}, \tag{21d}$$

where $d^{(2)}$ is the nonlinear coupling coefficient of the layer. SH fields generated in the forward and the backward directions are described respectively by the following expressions:

$$I_{2\omega}^{(+)} = \frac{2\omega^2}{c^3\epsilon_0}\left[\frac{d^{(2)}}{4}\left(1+\frac{3}{n^2}\right)\right]^2 L^2[I_{\omega}^{(+,\mathrm{pump})}]^2, \tag{22a}$$

$$I_{2\omega}^{(-)} = \frac{2\omega^2}{c^3\epsilon_0}\left[\frac{d^{(2)}}{4}\left(1-\frac{1}{n^2}\right)\right]^2 L^2[I_{\omega}^{(+,\mathrm{pump})}]^2. \tag{22b}$$

In Fig. 3, we show the forward and the backward conversion efficiencies plotted versus the input intensity for the single layer described in the caption of the figure. From Eqs. (22) we also obtain

$$\frac{I_{2\omega}^{(+)}}{I_{2\omega}^{(-)}} = \left(\frac{n^2+3}{n^2-1}\right)^2. \tag{23}$$

Equation (23) suggests that, in the limit of large n and strong feedback, forward and backward conversion efficiencies become approximately equal. In the case of SHG by counterpropagating pump beams, we obtain

$$I_{2\omega}^{(+)} = \frac{2\omega^2}{c^3\epsilon_0}\left[\frac{d^{(2)}}{4}\left(1+\frac{3}{n^2}\right)\right]^2 L^2[I_{\omega}^{(+,\mathrm{pump})}]^2 \times \left|1+Q\left(\frac{n^2-1}{n^2+3}\right)\exp(2i\,\delta\phi_{\omega}) + 2\sqrt{Q}\left(\frac{n^2-1}{n^2+3}\right)\exp[i(\delta\phi_{\omega}+m\pi)]\right|^2, \tag{24a}$$

$$I_{2\omega}^{(-)} = \frac{2\omega^2}{c^3\epsilon_0}\left[\frac{d^{(2)}}{4}\left(1-\frac{1}{n^2}\right)\right]^2 L^2[I_{\omega}^{(+,\mathrm{pump})}]^2 \times \left|1+Q\left(\frac{n^2+3}{n^2-1}\right)\exp(2i\,\delta\phi_{\omega}) + 2\sqrt{Q}\exp[i(\delta\phi_{\omega}+m\pi)]\right|^2, \tag{24b}$$

where $Q = I_{\omega}^{(-,\mathrm{pump})}/I_{\omega}^{(+,\mathrm{pump})}$ is the ratio between the RTL and the LTR input intensities and $\delta\phi_{\omega} = \gamma_{\omega}^{(-)} - \gamma_{\omega}^{(+)}$ is the phase difference of the input fields, as in Eqs. (19). From Figs. 4, one can deduce that the SHG process can be inhibited for a wide range of values of the phase difference $\delta\phi_{\omega}$. This inhibition makes it possible to achieve a sensitive phase-controlled, all-optical switching process. We say more about the possibility of controlling SH generation with counterpropagating beams in Section 6.

5. RESONANT INTERACTIONS IN FINITE, NONABSORBING, MULTILAYERED STRUCTURES

In the case of resonant interactions, i.e., when both the FF and the SH modes are tuned to transmission resonances, the coupled-mode equations (13) can be recast in

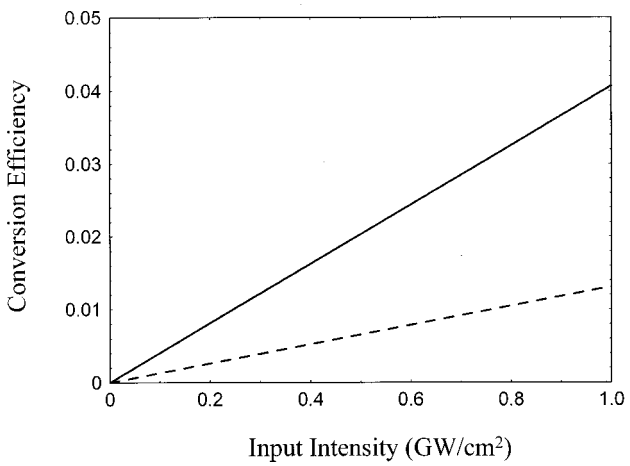

Fig. 3. Forward (solid curve) and backward (dashed curve) conversion efficiency, defined by $\eta^{(\pm)} = I_{\omega}^{(\pm)}/I_{\omega}^{(+,\mathrm{pump})}$, plotted versus the input pump intensity $I_{\omega}^{(+,\mathrm{pump})}$ for an undepleted pump, as given by Eqs. (22). The layer thickness is $L = 10\ \mu$m, the refractive index is $n = 2.5$, the nonlinear coefficient is taken to be equal to $d^{(2)} = 100$ pm/V. The wavelength of the pump beam is $\lambda = 1\ \mu$m, and the pump is tuned to the $m = 50$ transmission resonance.

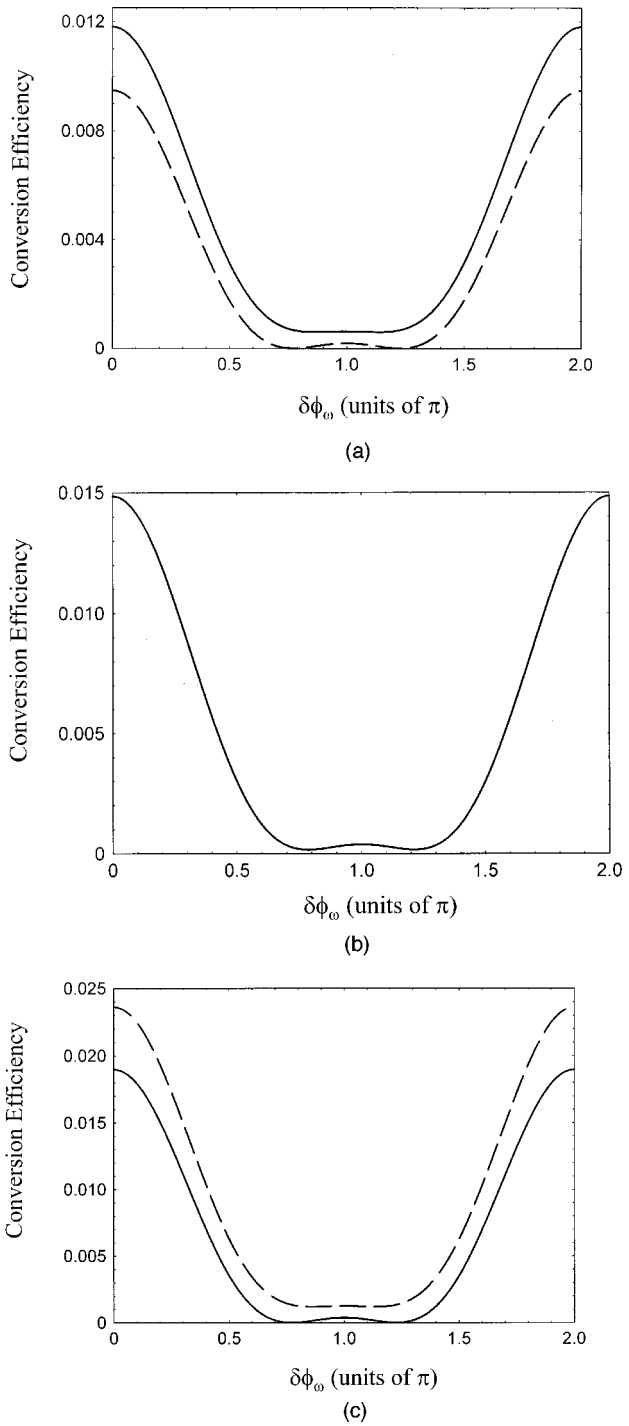

Fig. 4. Forward (solid curve) and backward (dashed curve) conversion efficiencies for $\eta^{(\pm)} = I_\omega^{(\pm)}/(I_\omega^{(+,\mathrm{pump})} + I_\omega^{(-,\mathrm{pump})})$ plotted versus the phase difference of the input fields $\delta\phi_\omega = \gamma_\omega^{(-)} - \gamma_\omega^{(+)}$ for different pump-intensity ratios $Q = I_\omega^{(-,\mathrm{pump})}/I_\omega^{(+,\mathrm{pump})}$. (a) $Q = 0.5$, (b) $Q = 1$, (c) $Q = 2$. For $Q = 1$ the forward and the backward conversion efficiency are equal. All the parameters are the same as reported in the caption of Fig. 3 and $I_\omega^{(+,\mathrm{pump})} = 0.1\ \mathrm{GW/cm^2}$.

a simpler form. Although it may seem draconian to restrict our discussion to transmission resonances, in reality off-resonant quadratic interactions become very inefficient for at least two reasons: (a) the impossibility of finding phase-matching conditions, and (b) poor field localization inside the structure, as outlined in Refs. 1, 2, and 7.

Let us begin by writing the LTR and the RTL modes as $\Phi_{j\omega}^{(\pm)}(z) = |\Phi_{j\omega}^{(\pm)}(z)|\exp[i\phi_{j\omega}^{(\pm)}]$. Because we are considering real grating profiles, it follows that $|\Phi_{j\omega}^{(\pm)} \times (z)|^2[\mathrm{d}\phi_{j\omega}^{(\pm)}/\mathrm{d}z]$ is a conserved quantity[16] that can be calculated by one's resorting to the boundary conditions imposed on the LTR and the RTL modes (see Fig. 2). At the peaks of transmission, where $r_{j\omega}^{(\pm)} = 0$, we obtain[16]

$$|\Phi_{j\omega}^{(\pm)}|^2 \frac{\mathrm{d}\phi_{j\omega}^{(\pm)}}{\mathrm{d}z} = \pm\frac{j\omega}{c}. \tag{25}$$

The boundary conditions on the LTR and the RTL modes are

$$\Phi_{j\omega}^{(+)}(0) = \Phi_{j\omega}^{(-)}(L) = 1, \tag{26a}$$

$$\Phi_{j\omega}^{(-)}(0) = \Phi_{j\omega}^{(+)}(L) = \exp[i\phi_t(j\omega)], \tag{26b}$$

where $\phi_t(j\omega)$ is the phase of the transmission function, $t_{j\omega} = (T_{j\omega})^{1/2}\exp[i\phi_t(j\omega)]$. It can be verified that, for nonabsorbing structures, $t_{j\omega}^{(+)} = t_{j\omega}^{(-)} = t_{j\omega}$ as a consequence of time-reversal symmetry. From Eqs. (25) and from the boundary conditions [Eqs. (26)], we obtain

$$p_{j\omega}^{(+,+)} = \langle\Phi_{j\omega}^{(+)}|\hat{p}_{j\omega}\Phi_{j\omega}^{(+)}\rangle = 1, \tag{27a}$$

$$p_{j\omega}^{(-,-)} = \langle\Phi_{j\omega}^{(-)}|\hat{p}_{j\omega}\Phi_{j\omega}^{(-)}\rangle = -1, \tag{27b}$$

$$p_{j\omega}^{(-,+)} = [p_{j\omega}^{(+,-)}]^* + \frac{2c}{j\omega L}\sin[\phi_t(j\omega)]. \tag{27c}$$

B. Symmetric Structures

For symmetric structures the amplitudes of the LTR and the RTL modes are equal: $|\Phi_{j\omega}^{(+)}| = |\Phi_{j\omega}^{(-)}|$. As a consequence, from Eqs. (25) and (26) we obtain

$$\Phi_{j\omega}^{(-)} = \Phi_{j\omega}^{(+)*}\exp[i\phi_t(j\omega)]. \tag{28}$$

Substituting Eq. (28) into the expressions for the off-diagonal elements of the momentum operator [see Eq. (14a)], integrating by parts, and using the boundary conditions given in Eqs. (26), we obtain

$$p_{j\omega}^{(-,+)} = -[p_{j\omega}^{(+,-)}] = \frac{c}{j\omega L}\sin[\phi_t(j\omega)]. \tag{29}$$

In the regime in which $\lambda \ll 2\pi L$ (λ is the wavelength of the FF field in vacuum), the off-diagonal elements of the momentum operator become negligible with respect to the diagonal elements, and the coupled-mode equations can be written in the following form:

$$\frac{\mathrm{d}A_\omega^{(+)}}{\mathrm{d}z} = i\frac{\omega}{c}\sum_{(k,l)=(+,-)}\Gamma_{(\omega,+)}^{(k,l)}A_{2\omega}^{(k)}A_\omega^{(l)*}, \tag{30a}$$

$$\frac{\mathrm{d}A_\omega^{(-)}}{\mathrm{d}z} = -i\frac{\omega}{c}\sum_{(k,l)=(+,-)}\Gamma_{(\omega,-)}^{(k,l)}A_{2\omega}^{(k)}A_\omega^{(l)*}, \tag{30b}$$

$$\frac{\mathrm{d}A_{2\omega}^{(+)}}{\mathrm{d}z} = i\frac{\omega}{c}\sum_{(k,l)=(+,-)}\Gamma_{(2\omega,+)}^{(k,l)}A_\omega^{(k)}A_\omega^{(l)}, \tag{30c}$$

$$\frac{dA_{2\omega}^{(-)}}{dz} = -i\frac{\omega}{c}\sum_{(k,l)=(+,-)}\Gamma_{(2\omega,-)}^{(k,l)}A_{\omega}^{(k)}A_{\omega}^{(l)}. \tag{30d}$$

The solutions for the case of a SH signal generated by counterpropagating pump beams in the undepleted pump regime can be written as

$$I_{2\omega}^{(+)} = \frac{2\omega^2}{c^3\epsilon_0}L^2[I_{\omega}^{(+,\mathrm{pump})}]^2|\Gamma_{(2\omega,+)}^{(+,+)}|^2 \times\left|1+Q\frac{\Gamma_{(2\omega,+)}^{(-,-)}}{\Gamma_{(2\omega,+)}^{(+,+)}}\exp(2i\delta\phi_{\omega}) + 2\sqrt{Q}\exp(i\delta\phi_{\omega})\frac{\Gamma_{(2\omega,+)}^{(+,-)}}{\Gamma_{(2\omega,+)}^{(+,+)}}\right|^2, \tag{31a}$$

$$I_{2\omega}^{(-)} = \frac{2\omega^2}{c^3\epsilon_0}L^2[I_{\omega}^{(+,\mathrm{pump})}]^2|\Gamma_{(2\omega,-)}^{(+,+)}|^2 \times\left|1+Q\exp(2i\delta\phi_{\omega})\frac{\Gamma_{(2\omega,-)}^{(-,-)}}{\Gamma_{(2\omega,-)}^{(+,+)}} + 2\sqrt{Q}\frac{\Gamma_{(2\omega,-)}^{(+,-)}}{\Gamma_{(2\omega,-)}^{(+,+)}}\exp(i\delta\phi_{\omega})\right|^2. \tag{31b}$$

In the case of generation by a single pump beam, i.e., $Q = 0$, the SH signal generated in the forward direction depends on the effective coupling coefficient

$$\Gamma_{(2\omega,+)}^{(+,+)} = (1/L)\int_0^L \Phi_{2\omega}^{(+)*}d^{(2)}(z)[\Phi_{\omega}^{(+)}]^2dz,$$

as is also predicted in Ref. 17 through more heuristic arguments and later experimentally verified in Refs. 6 and 7. The coupling coefficient $\Gamma_{(2\omega,+)}^{(+,+)}$ is a phase-dependent overlap integral whose magnitude is maximized when the fields overlap well inside the nonlinear material, i.e., when the fields coherently interact inside the structure.[17]

The perfect phase-matching conditions studied in Ref. 2 correspond to the case in which the effective coupling coefficient becomes an approximately real quantity, and its value is

$$\Gamma_{(2\omega,+)}^{(+,+)} \approx (1/L)\int_0^L d^{(2)}|\Phi_{2\omega}^{(+)}||\Phi_{\omega}^{(+)}|^2dz.$$

At the transmission resonance the DOM can be expressed as[7]

$$\rho_{\omega} = (1/Lc)\int_0^L \epsilon_{\omega}(z)|\Phi_{\omega}^{(+)}|^2dz.$$

It follows that $\Gamma_{(2\omega,+)}^{(+,+)}$ is enhanced by a factor proportional to the DOM when the LTR linear mode is localized inside the nonlinear layers, namely, $\Gamma_{(2\omega,+)}^{(+,+)} \propto \rho_{\omega}d_{\mathrm{layer}}^{(2)}$, where $d_{\mathrm{layer}}^{(2)}$ is the actual second-order susceptibility of the nonlinear layer.[7] This situation means that the conversion efficiency during a SHG process in a PBG structure is enhanced by a factor proportional to ρ_{ω}^2 with respect to an equivalent length of perfectly phase-matched bulk material. The DOM is proportional to N^2, where N is the number of periods[18]; this condition leads to SH conversion efficiencies proportional to factor of N^4 better when compared with an equivalent length of phase-matched bulk material. The conversion efficiency in a perfectly phase-matched PBG structure follows the scaling law η

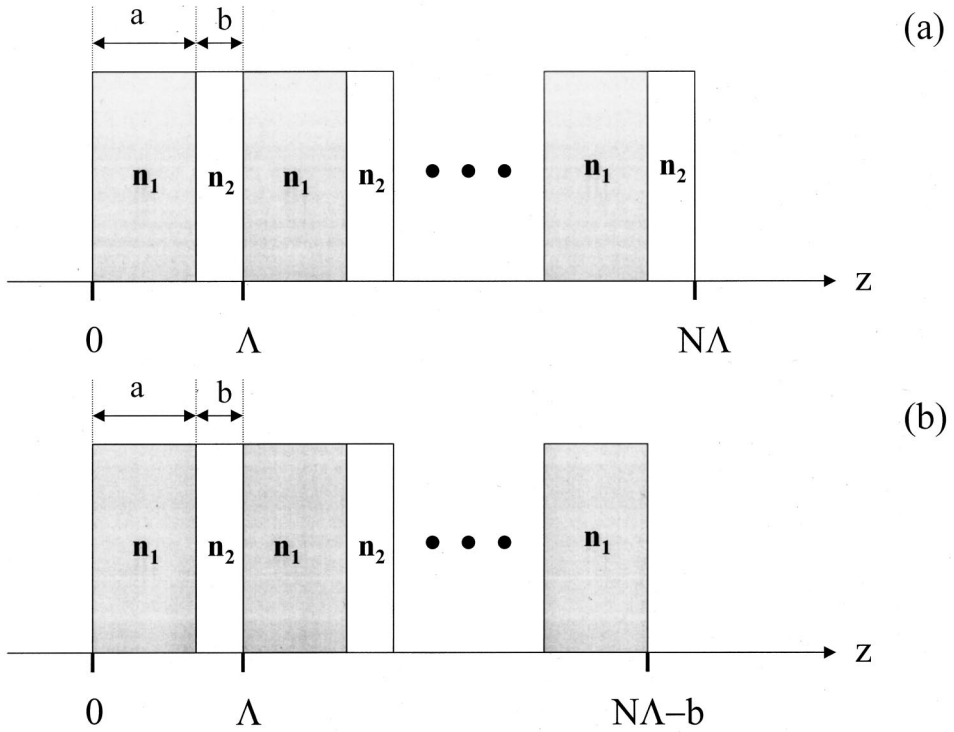

Fig. 5. (a) Generic N-period stack composed of two-layer unit cells of thicknesses a and b and constant, real indices n_1 and n_2, respectively. (b) Symmetry is restored to the structure by removing the last layer.

$\propto (\rho_\omega d^{(2)}_{\text{layer}} L)^2 \approx N^6$, as was analytically demonstrated first in Ref. 17. On the basis of these considerations it should be evident that the high DOM and the particular phase conditions that are available near the photonic band edge make PBG structures the best candidates for highly efficient, micrometer-sized devices based on quadratic nonlinearities.

C. Periodic Structures

The simplest example of a 1-D, periodic multilayered structure is that made by the repetition of a unit cell composed of two layers of refractive indices n_1 and n_2 taken N times the unit cell. The structure is illustrated in Fig. (5a). The optical properties of the periodic structure depicted in Fig. (5a) are approximately the same as those of the symmetric structure depicted in Fig. (5b), provided that the optical path of the last layer is negligible compared with the total optical path of the structure. More quantitatively, this relation means that $N(1 + n_1 a/n_2 b) \gg 1$. If this condition is satisfied both the LTR and the RTL linear modes possess approximately the same symmetry properties, as in Eq. (28): $\Phi^{(-)}_{j\omega} \approx \Phi^{(+)*}_{j\omega} \times \exp[i\phi_t(j\omega)]$. Therefore the off-diagonal elements of the momentum operator can be estimated as follows:

$$p^{(-,+)}_{j\omega} \approx -[\,p^{(+,-)}_{j\omega}] \approx \frac{c}{j\omega L}\sin[\,\phi_t(j\omega)]. \tag{32}$$

Once again, in the regime in which $\lambda \ll 2\pi L$, the off-diagonal elements of the momentum operator become negligible with respect to its diagonal elements, and the coupled-mode equations can be formally written in the same way as for symmetric structures:

$$\frac{dA^{(+)}_\omega}{dz} = i\frac{\omega}{c}\sum_{(k,l)=(+,-)} \Gamma^{(k,l)}_{(\omega,+)} A^{(k)}_{2\omega} A^{(l)*}_\omega, \tag{33a}$$

$$\frac{dA^{(-)}_\omega}{dz} = -i\frac{\omega}{c}\sum_{(k,l)=(+,-)} \Gamma^{(k,l)}_{(\omega,-)} A^{(k)}_{2\omega} A^{(l)*}_\omega, \tag{33b}$$

$$\frac{dA^{(+)}_{2\omega}}{dz} = i\frac{\omega}{c}\sum_{(k,l)=(+,-)} \Gamma^{(k,l)}_{(2\omega,+)} A^{(k)}_{\omega} A^{(l)}_\omega, \tag{33c}$$

$$\frac{dA^{(-)}_{2\omega}}{dz} = -i\frac{\omega}{c}\sum_{(k,l)=(+,-)} \Gamma^{(k,l)}_{(2\omega,-)} A^{(k)}_{\omega} A^{(l)}_\omega. \tag{33d}$$

In the undepleted pump regime, we obtain

$$I^{(+)}_{2\omega} = \frac{2\omega^2}{c^3\epsilon_0} L^2 [I^{(+,\text{pump})}_\omega]^2 |\Gamma^{(+,+)}_{(2\omega,+)}|^2 \times \left| 1 + Q\frac{\Gamma^{(-,-)}_{(2\omega,+)}}{\Gamma^{(+,+)}_{(2\omega,+)}}\exp(2i\,\delta\phi_\omega) + 2\sqrt{Q}\exp(i\,\delta\phi_\omega)\frac{\Gamma^{(+,-)}_{(2\omega,+)}}{\Gamma^{(+,+)}_{(2\omega,+)}}\right|^2, \tag{34a}$$

$$I^{(-)}_{2\omega} = \frac{2\omega^2}{c^3\epsilon_0} L^2 [I^{(+,\text{pump})}_\omega]^2 |\Gamma^{(+,+)}_{(2\omega,-)}|^2 \times \left| 1 + Q\exp(2i\,\delta\phi_\omega)\frac{\Gamma^{(-,-)}_{(2\omega,-)}}{\Gamma^{(+,+)}_{(2\omega,-)}} + 2\sqrt{Q}\frac{\Gamma^{(+,-)}_{(2\omega,-)}}{\Gamma^{(+,+)}_{(2\omega,-)}}\exp(i\,\delta\phi_\omega)\right|^2. \tag{34b}$$

6. SECOND-HARMONIC GENERATION IN A FINITE, NONABSORBING PHOTONIC BANDGAP STRUCTURE: COMPARISON WITH NUMERICAL RESULTS

Alternative options to the numerical integration of Eqs. (1) also exist in the form of more approximate solutions for the case of shallow gratings.[8,9] In this paper, we propose a simple and elegant approach that makes it possible to find analytical solutions for Eqs. (1) in many dynamical situations. Furthermore, the method that we propose can be applied to any generic linear index profile, provided the monochromatic regime is approached.

To test the validity of the model, we compare in Fig. 6 the conversion efficiency for the SH signal generated with a single pump beam, i.e., $Q = 0$, as calculated from Eqs. (31), with the results of the conversion efficiency calculated by numerical integration of the nonlinear coupled Maxwell equations in the time domain.[19] The structure under consideration is symmetric, and the details are described in the caption. The pump field at the wavelength of $\lambda = 1.69\ \mu$m is tuned at the first transmission resonance near the first-order bandgap, and the SH field is tuned at the second transmission resonance near the

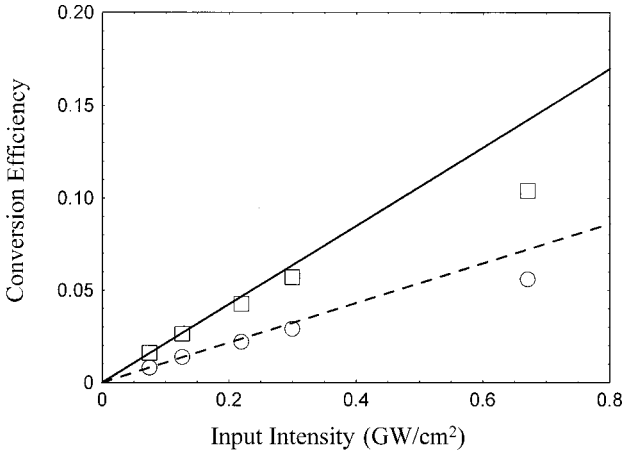

Fig. 6. Forward (solid curve) and backward (dashed curve) SH conversion efficiencies for $\eta^{(\pm)} = I^{(\pm)}_\omega / I^{(+,\text{pump})}_\omega$ plotted versus the input pump intensity as calculated from Eqs. (31) in the undepleted pump regime. Forward (squares) and backward (circles) conversion efficiencies were calculated by use of the algorithm of the fast Fourier transform beam-propagation method. The structure is the same as that described in the caption of Figs. 1. The nonlinear material is dispersed in the high-index layer, with $d^{(2)} = 80$ pm/V. The high-index material is also assumed to be dispersive, and its index of refraction at the SH frequency is $n_1(2\omega) = 1.5179$. The wavelength of the incident pump is $\lambda = 1.69\ \mu$m and is tuned to the first transmission resonance near the first-order bandgap.

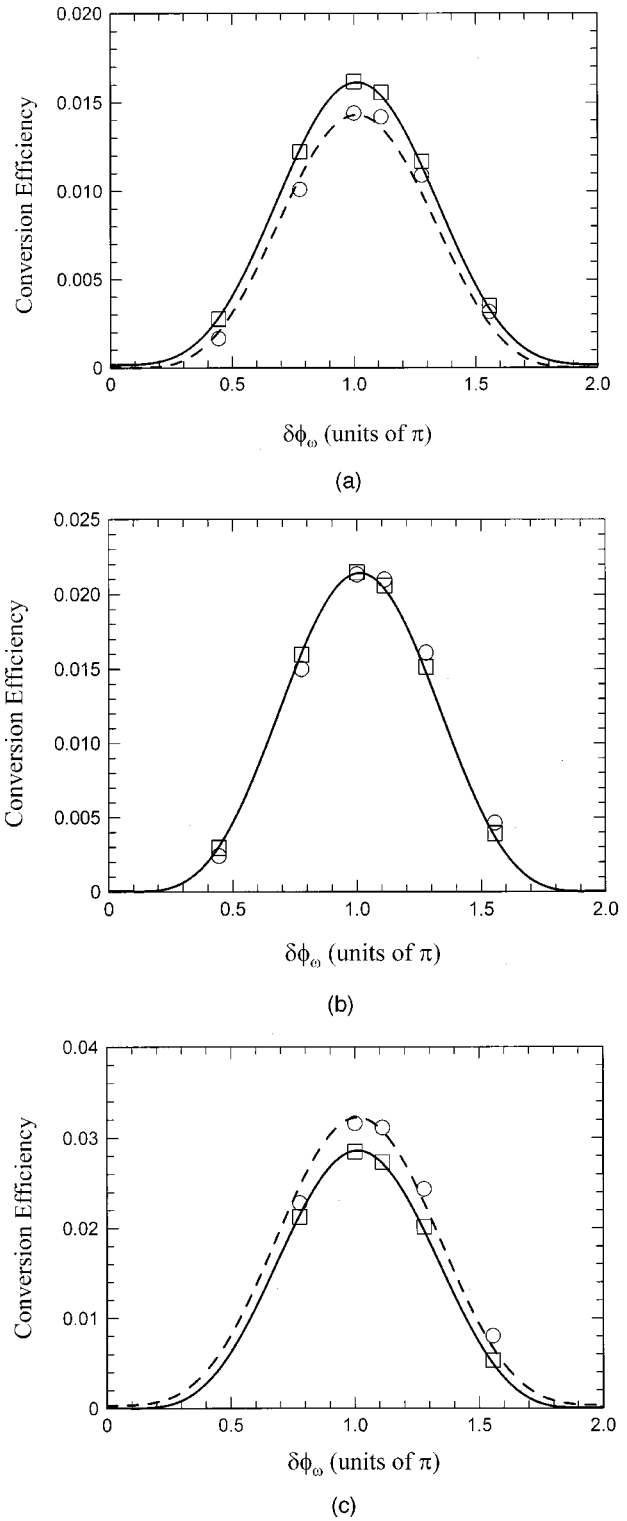

Fig. 7. Forward (solid curves) and backward (dashed curves) conversion efficiencies for $\eta^{(\pm)} = I_\omega^{(\pm)}/(I_\omega^{(+,\mathrm{pump})} + I_\omega^{(-,\mathrm{pump})})$ plotted versus the phase difference of the input fields $\delta\phi_\omega = \gamma_\omega^{(-)} - \gamma_\omega^{(+)}$, for different pump intensity ratios $Q = I_\omega^{(-,\mathrm{pump})}/I_\omega^{(+,\mathrm{pump})}$: (a) $Q = 0.5$, (b) $Q = 1$, (c) $Q = 2$. For $Q = 1$ the backward and the forward conversion efficiencies are equal. Forward (squares) and backward (circles) conversion efficiencies were calculated numerically. All the parameters are the same as those reported in the caption of Fig. 6, and $I_\omega^{(+,\mathrm{pump})} = 0.019\ \mathrm{GW/cm^2}$.

second-order bandgap. Under these tuning conditions the SH field is exactly phase matched with the FF field.[2] The nonlinear coefficient of the high index layer is $d^{(2)} = 80$ pm/V. Figure 6 suggests that both the forward and the backward conversion efficiencies predicted by Eqs. (31) are nearly indistinguishable from the numerical results in the undepleted regime—or at least for total conversion efficiencies that do not exceed approximately 10%. Therefore we conclude that, when pump depletion is negligible, one may describe the dynamics by straightforward numerical integration of the coupled-mode equations, i.e., Eqs. (30), by a shooting algorithm,[20] for example.

In Fig. 7, we plot the SH signal generated by counterpropagating beams as a function of the phase difference between the input pump fields and for different ratios of the input intensities. We note an interesting phenomenon: SH emission can be severely disrupted with a proper choice of the relative input phases of the incident beams. In particular, we point out that, even though the interaction takes place under exact phase-matching conditions, SH emissions are practically switched off when the phase differences are $0 \leqslant \delta\phi_\omega \leqslant \pi/4$ and $7/4\pi \leqslant \delta\phi_\omega \leqslant 2\pi$ (see Fig. 7). The contrast between the ON and the OFF states can be 2 to 4 orders of magnitude with respect to the maximum SH emission that occurs when $\delta\phi_\omega \cong \pi$. The possibility of controlling high-harmonic generation in gases by use of counterpropagating beams has recently been addressed in the literature.[21] Pattern-formation and -modulation instabilities resulting from the interaction of counterpropagating beams have recently been investigated for quadratic nonlinear media.[22] A comprehensive study of nonlinear interactions in PBG structures that are due to counterpropagating fields is beyond the scope of this study but will be given more attention in future investigations.

7. CONCLUSIONS

In summary, we have presented a generalized coupled-mode theory for quadratic interactions in multilayered structures of finite length. Because no assumptions have been made with regard to the type of grating, Eqs. (13) and (14) are valid for gratings of arbitrary depth and profile. We have exploited different interaction regimes and have derived simple analytical solutions for the case of SH generation under resonant conditions in nonabsorbing structures, as exemplified by our Eqs. (31). The results predicted by this theory are in excellent agreement with those obtained by use of a numerical integration of the nonlinear, coupled equations in the time domain. We believe that it may be possible to extend the present results to include at least one transverse dimension, which would make it possible to study diffraction and diffraction effects in general.

ACKNOWLEDGMENTS

We thank J. W. Haus and N. Mattiucci for interesting discussions. G. D'Aguanno and M. Centini thank the U.S. Army European Research Office for partial financial support (grant R&D 8766-PH-01).

G. D'Aguanno's e-mail address is giuseppe.daguanno @uniroma1.it.

REFERENCES AND NOTE

1. M. Scalora, M. J. Bloemer, A. S. Manka, J. P. Dowling, C. M. Bowden, R. Viswanathan, and J. W. Haus, "Pulsed second-harmonic generation in nonlinear, one-dimensional, periodic structure," Phys. Rev. A **56**, 3166–3174 (1997).
2. M. Centini, C. Sibilia, M. Scalora, G. D'Aguanno, M. Bertolotti, M. Bloemer, C. M. Bowden, and I. Nefedov, "Dispersive properties of finite, one-dimensional photonic bandgap structures: applications to nonlinear quadratic interactions," Phys. Rev. E **60**, 4891–4898 (1999).
3. A. V. Balakin, D. Boucher, V. A. Bushev, N. I. Koroteev, B. I. Mantsyzov, P. Masselin, I. A. Ozheredov, and A. P. Shurinov, "Enhancement of second-harmonic generation with femtosecond laser pulses near the photonic band edge for different polarizations of incident light," Opt. Lett. **24**, 793–795 (1999).
4. G. D'Aguanno, M. Centini, C. Sibilia, M. Bertolotti, M. Scalora, M. Bloemer, and C. M. Bowden, "Enhancement of $\chi^{(2)}$ cascading processes in one-dimensional photonic bandgap structures," Opt. Lett. **24**, 1663–1665 (1999).
5. Y. Dumeige, P. Vidakovic, S. Sauvage, I. Sagnes, J. A. Levenson, C. Sibilia, M. Centini, G. D'Aguanno, and M. Scalora, "Enhancement of second harmonic generation in a 1-D semiconductor photonic bandgap," Appl. Phys. Lett. **78**, 3021–3023 (2001).
6. M. Scalora, M. J. Bloemer, C. M. Bowden, G. D'Aguanno, M. Centini, C. Sibilia, M. Bertolotti, Y. Dumeige, I. Sagnes, P. Vidakovic, and A. Levenson, "Choose your color from the photonic band edge: nonlinear frequency conversion," Opt. Photon. News **12**, 36–40 (2001).
7. G. D'Aguanno, M. Centini, M. Scalora, C. Sibilia, Y. Dumeige, P. Vidakovic, J. A. Levenson, M. J. Bloemer, C. M. Bowden, J. W. Haus, and M. Bertolotti, "Photonic band edge effects in finite structures and applications to $\chi^{(2)}$ interactions," Phys. Rev. E **64**, 016609–016619 (2001), and references therein.
8. J. W. Haus, R. Viswanathan, M. Scalora, A. G. Kalocsai, J. D. Cole, and J. Theimer, "Enhanced second-harmonic generation in media with weak periodicity," Phys. Rev. A **57**, 2120–2128 (1998), and references therein.
9. M. J. Steel and C. M. de Sterke, "Second-harmonic generation in second-harmonic fiber Bragg gratings," Appl. Opt. **35**, 3211–3222 (1996).
10. C. M. de Sterke and J. E. Sipe, "Envelope-function approach for the electrodynamics of nonlinear periodic structures," Phys. Rev. A **38**, 5149–5165 (1988).
11. A. Arraf and C. M. de Sterke, "Coupled-mode equations for quadratically nonlinear deep gratings," Phys. Rev. E **58**, 7951–7958 (1998), and references therein.
12. T. Iizuka and C. M. de Sterke, "Corrections to coupled mode theory for deep gratings," Phys. Rev. E **61**, 4491–4499 (2000).
13. O. Di Stefano, S. Savasta, and R. Girlanda, "Mode expansion and photon operators in dispersive and absorbing dielectrics," J. Mod. Opt. **48**, 67–84 (2001).
14. P. Yeh, *Optical Waves in Layered Media* (Wiley, New York, 1988).
15. A. Nayfeh, *Introduction to Perturbation Techniques* (Wiley, New York, 1993).
16. G. D'Aguanno, M. Centini, M. Scalora, C. Sibilia, M. J. Bloemer, C. M. Bowden, J. W. Haus, and M. Bertolotti, "Group velocity, energy velocity and superluminal propagation in finite photonic bandgap structures," Phys. Rev. E **63**, 036610–036615 (2001).
17. G. D'Aguanno, "Nonlinear $\chi^{(2)}$ interactions in bulk and stratified materials," Ph.D. Thesis (National Library of Italy, Rome, 1999) pp. 72–78.
18. J. M. Bendickson, J. P. Dowling, and M. Scalora, "Analytic expression for the electromagnetic mode density in finite, one-dimensional, photonic bandgap structures," Phys. Rev. E **53**, 4107–4121 (1996).
19. The numerical calculations were performed by use of a fast Fourier transform beam-propagation method that integrates the equations of motion in the time domain, as outlined in Ref. 1. Incident pulses are assumed to be 2 ps in duration and have the following intensity profile in time: $I^{(\text{pump})}(t) = I^{(\text{peak})} \exp[-(t^2/2\sigma^2)]$, where $I^{(\text{peak})}$ is the peak intensity of the pump. A comparison with plane-wave results by use of pulses is possible because the spatial extension of these pulses is nearly 3 orders of magnitude greater than the structure length. As far as the structure is concerned, this incident pulse is nearly monochromatic, and the dynamics yield results that are nearly identical to the plane-wave results, provided the intensity of the plane wave is properly averaged over the pulse width. The average intensity of an incident plane-wave pump field is defined as
$$I^{(\text{pump})} = \frac{I^{(\text{peak})}}{4\sigma} \int_{-\infty}^{+\infty} \exp\left(-\frac{t^2}{2\sigma^2}\right) dt = (\pi/8)^{1/2} I^{(\text{peak})}.$$
20. W. H. Press, B. P. Flannery, S. A. Teukolsky, and W. T. Vetterling, *Numerical Recipes in C* (Cambridge U. Press, Cambridge, 1988).
21. S. L. Voronov, I. Kohl, J. B. Madsen, J. Simmons, N. Terry, J. Titensor, Q. Wang, and J. Peatross, "Control of laser high-harmonic generation with counterpropagating light," Phys. Rev. Lett. **87**, 133902–133914 (2001), and references therein.
22. P. M. Lushnikov, P. Lodahl, and M. Saffman, "Transverse modulational instability of counterpropagating quasi-phase-matched beams in a quadratically nonlinear medium" Opt. Lett. **23**, 1650–1652 (1999), and references therein.